

Molecular simulation of surface reorganization and wetting in crystalline cellulose I and II

Reinhard J. Maurer

*Department Chemistry, Technical University Munich,
Lichtenbergstr. 4, D-85747 Garching, Germany*

Alexander F. Sax* and Volker Ribitsch

*Department of Chemistry, University of Graz,
Heinrichstr. 28, A-8010 Graz, Austria*

Abstract

Cellulose is one of the most versatile substances in the world. Its immense variety of applications was in recent years complemented by nanotechnological applications such as cellulose nanoparticle dressed surfaces for filtration purposes or cellulose matrices for microelectronics. The fabrication of such complex materials asks for thorough understanding of the surface structure and its interactions with adsorbates. In this study we investigate several surface model systems of nanotechnological interest, which are obtained by reorganization of the cellulose-vacuum or cellulose-water interfaces of slabs of crystalline cellulose. To do this, we equilibrated first bulk supercells of different cellulose allomorphs, which were constructed from crystallographic data, and then optimized the interface structures. From the bulk and surface systems we calculated structural properties such as unit cell parameters, dihedral conformation distributions, density profiles and hydrogen bonding. The results suggest that no overall geometrical restructuring occurs at the interface. However, the hydrogen bond network is strongly reconstructed, as is inferred from the dihedral conformations and hydrogen bond occurrences, although only within the first few layers. This holds for low index close packed structures as well as for high index loosely packed surfaces. Replacing the vacuum by ambient pressure water molecules we find less rearrangements of the cellulose surface, because the water allows formation of hydrogen bonds similar to those in the bulk phase. The water near the cellulose surface shows, however, strong structural changes. We observe reduced mobility of the water molecules, which corresponds to a cooling of water by about 30 degrees, in a slab that is about 10 Å thick. Although structuring and adsorption is observed on all surfaces, no actual penetration of water into the cellulose structure could be observed. This suggests that pure water is not sufficient to produce cellulose swelling at mesoscopic timescales. This work lays the basis for current quantum chemical investigations on specific interaction terms within cellulose.

* alexander.sax@uni-graz.at

I. INTRODUCTION

Cellulose is one of the most abundant materials on earth [1]. Exploitation of the vast amount of this renewable substance dates back until ancient times. The recent uprising of nanotechnology has opened a new range of applications for cellulose and its derivatives. It is used for cellulose nanocomposites, such as flexible, transparent matrices for organic light emitting diodes (OLED) [2], or stable cellulose nanoparticles [3]. To obtain new smart materials the surface properties of crystalline cellulose must be properly modified. The importance of this branch of carbohydrate research has been underlined by approval of a research proposal within the European Union 7th framework program, called SURFUNCCELL, wherein 15 academic and industrial partners try to formulate nanostructured cellulose coatings with a variety of proposed applications, *e.g.* self cleaning surfaces or waste water treatment.

A systematic formulation of technologically interesting materials such as the one planned in the mentioned project needs deep understanding of the underlying molecular structure of and reactivity at surfaces of the solid phases. This is, however, complicate because cellulose is a polymorph with several crystalline forms such as $I\alpha$, $I\beta$, II, III, but also amorphous forms [1], which are partly coexistent. Cellulose is built from $\beta(1 \rightarrow 4)$ glucan molecules which are linear chains of D-glucose monomers linked by glycosidic bonds. In the two allomorphs $I\alpha$ and $I\beta$ of native cellulose all chains are parallel aligned having the same growth direction, the allomorphs differ in their crystal structures: $I\alpha$ has a triclinic unit cell of $P1$ symmetry with a single cellobiosyl unit as basis, the crystal consists of parallel layers of one type, $I\beta$ has a monoclinic unit cell of $P2_1$ symmetry with two cellobiosyl units as basis, termed origin and center, accordingly the crystal is made of two different alternating sheets. Regenerated cellulose II has a monoclinic unit cell of $P2_1$ symmetry with two cellobiosyl units. [4] Cellulose III is obtained when either cellulose I or cellulose II is treated with liquid ammonia, the resulting allomorphs are consequently denoted as III_1 or III_2 , both allomorphs are believed to have $P2_1$ unit cells. [5] This transformation is reversible. Heating of cellulose III leads to cellulose IV_1 and IV_2 , respectively, which can reversibly be transformed into cellulose I and II, respectively, both allomorphs have a P_1 unit cell.

The fact that native cellulose is composed of crystalline and amorphous domains makes

the structural investigation very complicated. Nonetheless, many different X-ray structures of cellulose were published over the years [4, 6–10]. These reports gave a very fundamental understanding of the molecular structure, but many structural aspects are inaccessible by X-ray diffraction, such as the hydrogen bond (HB) network or the structure of cellulose surfaces or interfaces between different phases.

Molecular modeling and especially molecular dynamics (MD) represent reliable tools to investigate structural and dynamical properties based on preliminary experimental results. Considering polysaccharides [11] and in particular cellulose many different modeling approaches are presented in literature, reaching from studies of bulk properties [11–15], thermal response [16], relative stability [17, 18] and deformation [19], to studies of solvated crystallites [20–22], surfaces properties or interaction with water [23–26] and adsorbates [27].

Films of regenerated cellulose are semicrystalline or amorphous, that means that highly ordered crystalline domains of cellulose II coexist with disordered domains within their elementary supramolecular units. Crystalline and amorphous cellulose differ in many physical and chemical aspects, amorphous cellulose is, for example, accessible to water, in contrast to crystalline cellulose.[28] Since most chemistry with cellulose is done in aqueous solutions, understanding of surface processes like adsorption needs a detailed knowledge of properties of the cellulose-water interface, however, little data on the crystalline ordering and crystal structure of cellulose films are available.[29] Modeling of the heterogenous surface structure of cellulose films is, therefore, rather difficult, it is more difficult for the amorphous than for the crystalline domains. When the crystalline domains are treated as crystallites the surfaces are best described by crystal planes; modeling of amorphous domains that are accessible to water can in principle be done with very large supercells and very irregular surfaces, but there are no data available, which can be used for modeling these surfaces. It is assumed that initial solubilization processes with water are only possible when many polar groups are exposed at the surfaces and when the surfaces area is maximal. In order to investigate surface reorganization of cellulose we choose surfaces generated from large Miller index crystal planes and compare them with low index surfaces. We specifically address the reconstruction of the cellulose/vacuum and cellulose/water interfaces and the influence of the surface morphology on the properties of the water component.

II. METHODS

Throughout this study, molecular dynamics (MD) and optimization runs were performed with the DL_POLY 2.20 package [30] using periodic boundary conditions. We used the all atom force field GLYCAM06 (Glycam06f.dat)[31] to describe the cellulose crystal systems and a non-rigid TIP3P model [32] to describe the water molecules. For the system setup we used AmberTools 11 [33] and ChemShell 3.3.1 [34], therewith producing DL_POLY readable force field files. Manipulations on the molecules were done using the model builder Aten [35], and visualization with VMD 1.8.6 [36]. Calculations were performed on an AMD64 Linux 24 node cluster with double precision.

All surface models are derived from the respective optimized bulk models, therefore, we first optimized the bulk properties of the investigated allomorphs. Each bulk model is represented by supercells which are repeats of the respective unit cells. The $I\alpha$ supercell has $5 \times 4 \times 5$ repeats of the triclinic unit cell and the $I\beta$ supercell has $2 \times 5 \times 5$ repeats of the monoclinic unit cell along the corresponding \vec{a} , \vec{b} and \vec{c} directions. The cellulose II (010) surface model is based on a bulk model which has $5 \times 2 \times 5$ repeats of the monoclinic unit cell, termed IIa. Unit cell parameters and coordinates of the cellobiose units were taken from recent X-ray diffraction studies[8–10]. All three systems contained 4200 atoms and their volume was about 33 nm³. The cell parameters are the respective X-ray values in Table 1. For the cellulose II (120) surface model we constructed a second bulk supercell IIb with $2 \times 2 \times 4$ repeats of a unit cell with 8 cellobiose units ($a = 29.27$ Å, $b = 8.93$ Å, 10.36 Å, $\alpha = \beta = 90^\circ$, $\gamma = 80.15^\circ$) 5376 atoms in a volume of 44 nm³. (*cf.* Fig. 1)

These systems were equilibrated and optimized in sequences of molecular dynamics and geometry optimizations, similar to a simulation protocol of [13]: 20 ps NVT MD at 600 K, geometry optimization, 20 ps NPT MD at 450 K, geometry optimization, 200 ps NPT MD at 300 K, geometry optimization. For the bulk models of cellulose II this sequence was preceded by a 40 ps N σ T MD at 300 K and geometry optimization.

The surface models are represented by slabs which consist of the corresponding optimized bulk supercells augmented by a vacuum slab of the same size. To model the $I\alpha$ (100), $I\beta$ (100), II (010) and the II (120) surfaces we thus doubled the size of our bulk supercells in one direction which was the b , a , b and b direction, respectively. All modeled systems consist of 4 sheets of cellulose chains parallel to the respective surfaces, with the lowest cellulose sheet

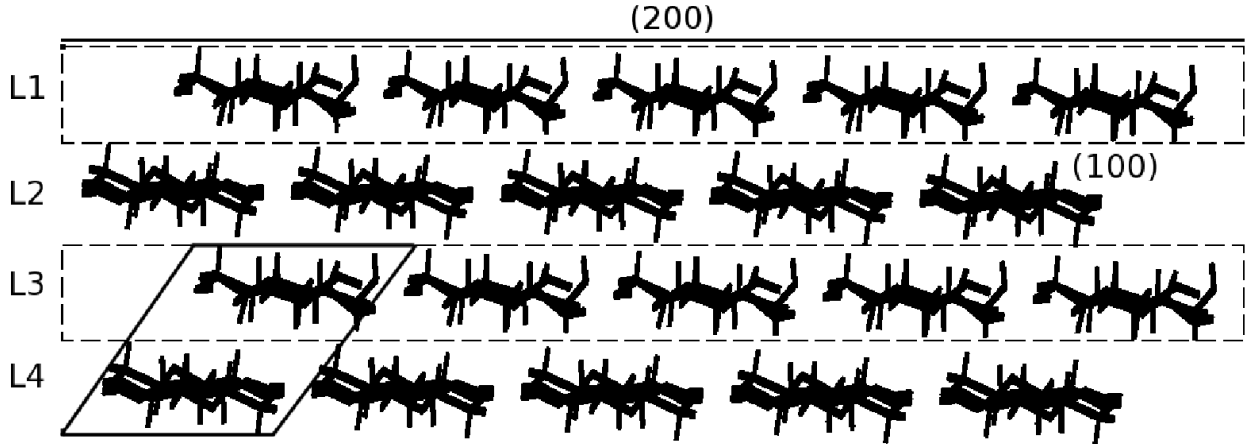


FIG. 1. Schematic representation of a cellulose I β surface. The small parallelogram at the left bottom depicts the unit cell of the system. The sheets are separated by dashed lines and defined as slabs of cellulose chains orthogonal to the envisaged surface (represented by the black line at the top). In this case the sheets defined by the elementary cell also act as layers in the slab.

being frozen to simulate a bulk boundary. To find out, whether this choice of slab is a too severe size limitation we performed some test calculations on cellulose I β and IIa with up to 8 sheets but did not find significant differences with respect to the measured observables, therefore the system size was restricted to 4 sheets throughout this study.

The surface/vacuum systems were equilibrated by the sequence: 20 ps NVT MD at 600 K, geometry optimization, 200 ps NPT MD at 300 K, geometry optimization.

For the surface/water systems we started from the respective optimized surface/vacuum systems where the vacuum slab was replaced by a 22 Å thick layer of water (density $\rho = 1 \text{ g cm}^{-3}$). The layer of water was built using the tool Packmol[37]. The systems were treated as follows: geometry optimization, 500 ps NVT MD at 300 K, geometry optimization.

All molecular dynamics runs were performed using a 1 fs time step, Ewald summation and Nose-Hoover thermostats and barostats with relaxation times $\tau_t = 0.1 \text{ ps}$ and $\tau_p = 1 \text{ ps}$. Observed quantities for bulk and surface systems were averaged over the last 100 ps of the corresponding 300 K MD run.

The self-diffusion coefficients for water were calculated using the Einstein relation. The mean-squared displacement data were averaged over the last 200 ps of the trajectory. The short averaging time does not allow an error estimate, but averaging over a significantly

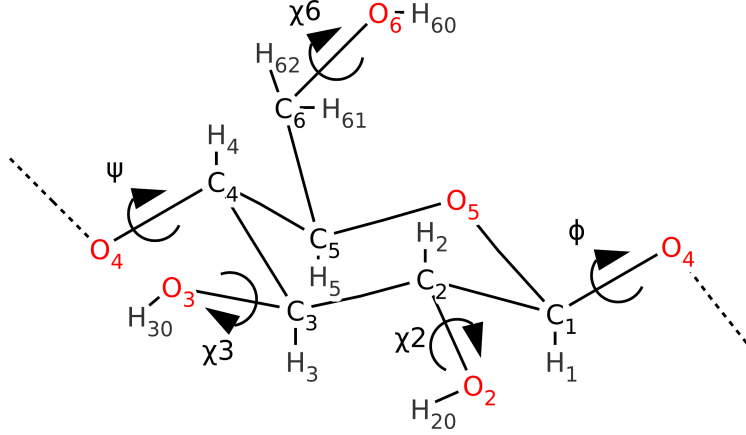


FIG. 2. GLYCAM06 naming convention used in this work.

longer run did not show any qualitative changes to the results.

In this work we use the GLYCAM06 [31] naming convention for glucose residues (Fig. 2).

III. RESULTS AND DISCUSSION

Bulk systems

Starting from the experimental structures obtained from X-ray diffraction, we equilibrated the bulk systems according to the scheme described in section II. Only few of the relaxed cell parameters listed in Table I differ considerably from the experimental cell parameters. We find an increase of the cell volume by about 5% with respect to the X-ray structures, which is mainly caused by the much larger c parameter, whereas the a and b parameters as well as the cell angles are very close to the experimental starting values. The reason for the larger c parameters is probably the underestimation of the puckering of the glucose rings by the force field resulting in flatter pyranose rings and, therefore, longer glucan chain. This seems to be a general problem of force fields as comparison with the results of other modeling studies for cellulose I β shows (see Table I).

A very recent study by Zhang *et al.*[38] investigated, using MD simulation in the NPT ensemble and the GLYCAM06 force field, the structural response of crystalline I β to heating from room temperature to 600 K. Experimentally, the change from a low temperature structure to a high temperature structure is found to be reversible, but in their MD simulation

TABLE I. Unit cell parameter of N σ T equilibrated systems (this study), and values from the literature. Experimental studies are marked with Exp.

Crystal phase	Study	a [Å]	b [Å]	c [Å]	α [deg]	β [deg]	γ [deg]	V[Å ³]
Cellulose I α	This Study	6.89(3)	5.83(3)	10.75(1)	120.4(4)	110.6(4)	81.7(3)	348.3
	[10] (Exp)	6.717	5.962	10.400	118.08	114.8	80.37	333.3
Cellulose I β	This Study	7.90(3)	8.40(1)	10.75(1)	85.1(2)	90.2(4)	102.2(5)	694.6
	[9] (Exp)	7.784	8.201	10.380	90	90	96.5	658.3
	[13]	8.378	8.168	10.523	89.97	89.97	90.92	720.0
	[20]	8.47	8.11	10.51	90	90	90	721.9
	[38], 298 K	7.63	8.23	10.80	89.99	89.99	97.17	672.9
	[38], 500 K	8.11	8.28	10.78	90.00	89.96	98.33	716.2
Cellulose IIa	This Study	8.02	9.32	10.77	90.2	91.6	121.5	686.1
	[4] (Exp)	8.01	9.04	10.36	90	90	117.1	667.8
	[8] (Exp)	8.10	9.05	10.31	90	90	117.1	672.8
Cellulose IIb	This Study	8.30	8.77	10.73	89.7	91.2	117.1	694.1

the phase transition was irreversible. The parameters of the unit cell for both structures in Table I show mainly an increase in the a parameter and a slight increase of γ , giving an increase of the volume of the unit cell.

Chen *et al.* [39] found the same irreversible change from the low to the high temperature structure in a simulation with the united atoms force field GROMOS 53a6 and attributed this fault to the parameters of the torsion potential for the exocyclic hydroxymethyl group. With properly changed potential parameters the phase transition became reversible.

There is no full agreement between our cell parameters for I β and those by Zhang *et al.*, but this is not surprising, because Zhang *et al.* systematically heated the system from room temperature to 500 K, whereas in the mixture of MD runs and geometry optimization described above for the equilibration of the bulk systems the highest temperature was 600 K. Moreover, the super cell we used had different size and shape. Our a parameter is in-between the corresponding low and high temperature values of Zhang *et al.*, the c parameters agree very well as do the β values. Our b value is closer to the high temperature value, our α value is by 5 degrees smaller than both values by Zhang *et al.*, and our γ value is 4 and

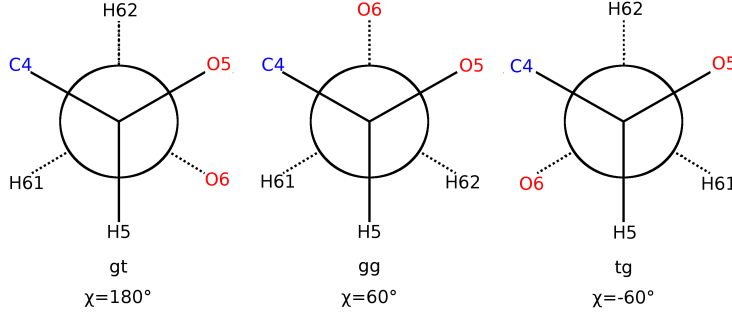


FIG. 3. Different conformations of C6 group. χ is defined as C4-C5-C6-O6 dihedral angle.

5 degrees larger than the high and low temperature values by Zhang *et al.*, the volume of our elementary cell is in-between the low and high temperature values. We assume that the equilibrated bulk cell obtained with our scheme is neither a full low temperature nor a full high temperature structure.

The phase transition is accompanied by a change in the conformation of the exocyclic hydroxymethyl group, which can be found in three staggered conformations termed *gg*, *gt* and *tg* where the first *g* and *t* mean gauche and trans position, respectively, of the C6-O6 group with respect to C5-O5, whereas the second *g* and *t* mean gauche and trans position of the C6-O6 group with respect to C5-C4. The conformations can be characterized by, e. g., the values of the C4-C5-C6-O6 dihedral angle χ (Figure 3). In the *tg* and *gt* conformations the position of the C6-O6 bond is equatorial with respect to the glucose six ring, in the *gg* conformation the C6-O6 bond is axial. In the *tg* conformation can accordingly the O6H group participate in intra- and inter-chain hydrogen bonds, in the *gt* conformation it participates only in interchain hydrogen bonds and in the *gg* conformation the O6H group can participate only in inter-sheet hydrogen bonds. Zhang *et al.* found that upon heating *tg* conformations in the origin sheets are dominantly changed into *gt* conformations, but into *gg* conformations in the center sheets.[38] Chen *et al.* [39] showed that above 500 K the *tg* conformations are completely replaced by *gt* and *gg* conformations.

Figure 4 shows the distribution of the hydroxymethyl conformations in the 4 cellulose systems investigated. In $I\beta$ the ration of *tg* : *gt* : *gg* is 38 : 31 : 31, so our $I\beta$ system is neither the low temperature system with 100 percent *tg*, nor is it the high temperature system with no *tg* conformations at all. The equal population of *gt* and *gg* conformations is in accord with the findings of Zhang *et al.* and Chen *et al.* Considering the influence

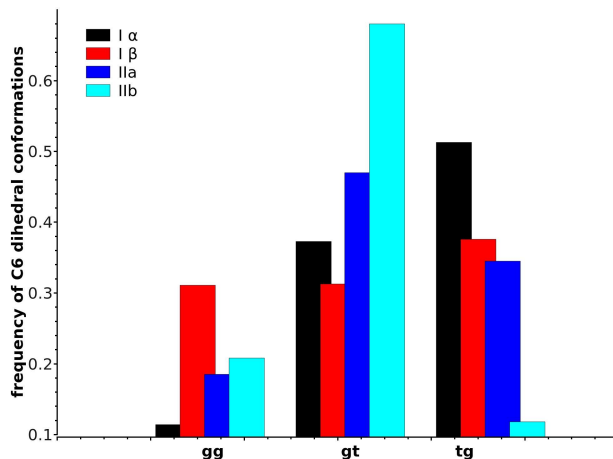


FIG. 4. Frequency of the hydroxymethyl conformations.

of the force field on the population of the hydroxymethyl conformations, one can assume that the high *gt* population in I α is also an artefact of the force field, the extremely low *gg* population is in agreement with experimental findings.

For the investigation of cellulose II we used two different supercells, the distribution of the hydroxymethyl conformations differs considerably for the *gt* and *tg* conformations: in both systems *tg* dominates but in IIa the percentage is below 50 percent and in IIb it is about 66 percent. In both systems the *gg* population is about 20 percent. We assume that the difference is caused by the equilibration scheme and the different size and shape of the supercells.

Hydrogen bonds in cellulose bulk

A hydrogen bond (HB) is a system where a hydrogen atom is covalently bonded to a donor oxygen OD-H bond, which weakly interacts with the lone pair electrons of an acceptor oxygen atom OA, that is not directly bonded to the group. Such a HB is represented by ODH...OA. Since the OH bond lengths in different HBs are rather constant, the non-bonded O...H distance and the OH...O angle are sufficient to characterize a HB.

Two types of intra-chain HBs between glucose rings can be found in a glucan molecule; the first one is O3-H...O5 with the hydroxyl group O3H in one glucose ring and the acceptor atom O5 in the next glucose ring; the second HB is O2-H...O6 with the hydroxyl group

TABLE II. Distribution of hydrogen bonds in I α bulk together with HB parameters. Only hydrogen bonds with a percentage higher than 0.5 are shown. Distances are given in Ångstrom, angles in degree.

HB	type ^a	rel. occ.	$d(\text{O} \cdots \text{HO})$	$\angle(\text{OHO})$
O5 \cdots HO3	A	32	1.86	155
O6 \cdots HO2	E	32	1.88	153
O6 \cdots HO3	E	1	2.06	159
O3 \cdots HO6	E	16	1.91	157
O2 \cdots HO6	A	16	1.93	159
O2 \cdots HO3	A	1	2.09	146
O4 \cdots HO6	S	1	2.01	153

^a) A means intra- and E means inter-chain, and S means inter-sheet hydrogen bonds.

O2-H in one ring and the acceptor atom O6 in the second ring. This HB is only possible when the exocyclic hydroxymethyl group has *tg* conformation. Thus, the covalent glycosidic bond and the two HBs build a strong link between two glucose rings and make the chain rather stiff. Interchain HBs connect glucan molecules to sheets, which interchain HBs are formed depends on the crystal structure and on the temperature.

Table II shows the relative occurrence of the different HBs in the equilibrated I α bulk.

Most important are the intra-chain HB O3H...O5 and the inter-chain HB O2H...O6; with 32 percent each, they represent nearly two third of the hydrogen bond network in the bulk, to the remaining third contribute the intra-chain HB O6H...O2 HB and the O6H...O3 inter-chain HB with about 16 percent each. That means, about half of the hydroxymethyl groups are found in the *tg* and the other half in the *gt* conformation. The rest of the HBs are weak intra-chain and inter-sheet HBs.

Crystalline cellulose I β is made of two alternating sheets (Figure 5) corresponding to the two different cellobiosyl units in the unit cell, called center and origin units. In one sheet the chains are nearly coplanar, in the other sheet the chains are slanted, Heiner *et al.* [23, 40] called these sheets "odd" and "even", we prefer "flat" and "rippled". According to authors like Nishiyama *et al.* [10] the origin units create the flat sheets others like Zhang *et al.* [38] make the flat sheet with the center units. Nishiyama *et al.* [9] showed for the first time the existence of different HB networks in the two sheets, Figure 5 visualizes the different HB

pattern.

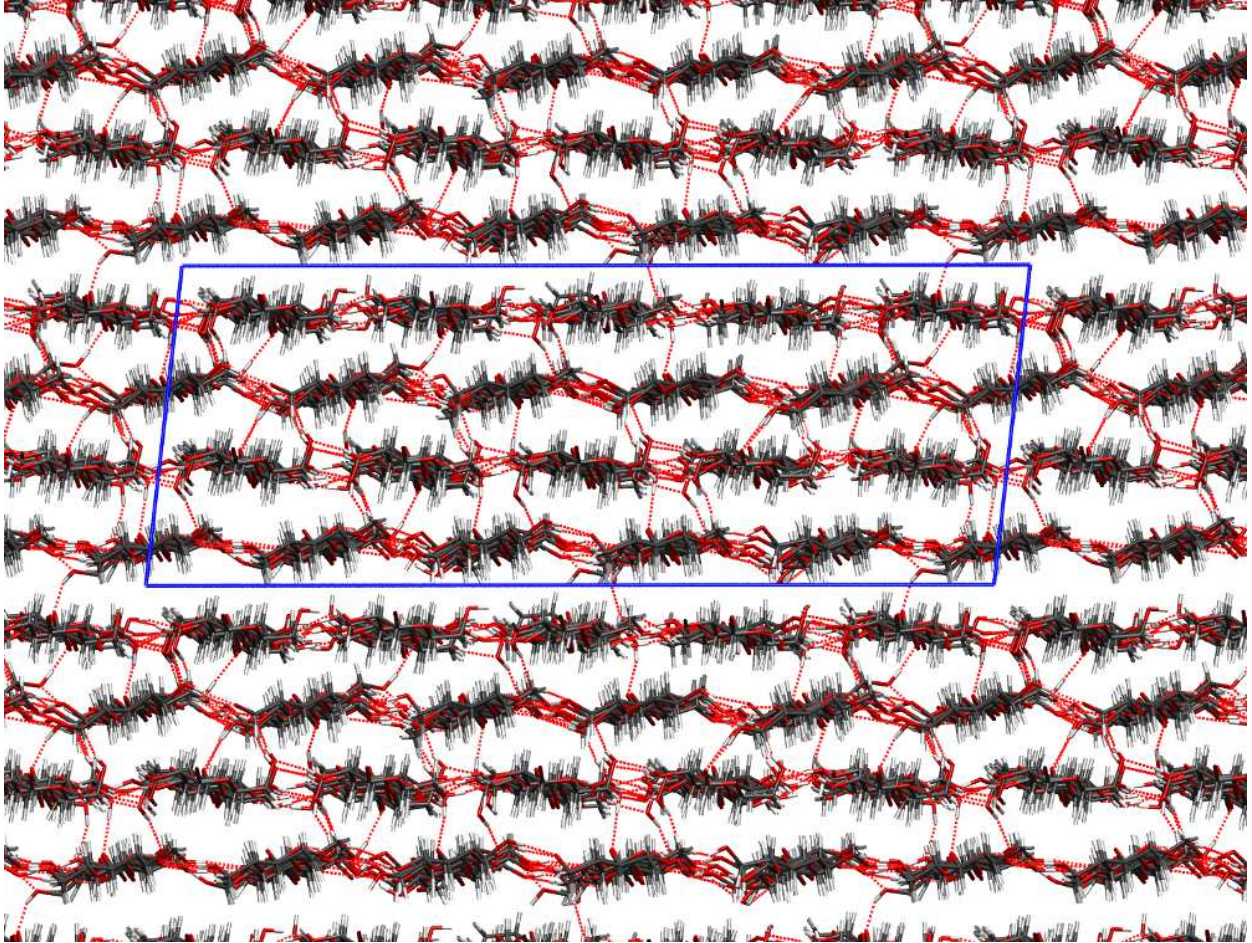


FIG. 5. a,b base plane projection of the cellulose $I\beta$ (100) slab.

The analysis of the HB network in equilibrated $I\beta$ bulk shows that in the rippled sheets there are about 20 percent more HBs than in the flat sheets, which corroborates the existence of two different HB networks. A detailed comparison of the two networks reveals equal numbers of intra-chain HBs O3H..O5 and inter-chain HBs O2H..O6 in both sheet types, these two HBs form the equal backbone of the HB networks. The difference between the two sheet types comes from the different numbers of O6H..O3 inter-chain HBs, which is in the rippled sheets about 2 to 3 times higher than in the flat sheets. That means, the stiffer chains in the flat sheets are connected mainly by O2H..O6 inter-chain HBs, the less stiff chains in the rippled sheets are connected by the same number of inter-chain HBs O2H..O6 and by additional O6H..O3 inter-chain HBs.

Compared with $I\alpha$, the number of *tg* conformations of the hydroxymethyl group decreases

TABLE III. Distribution of HBs in $I\beta$ bulk together with HB parameters. Only bonding atoms with a percentage higher than 0.5 are shown.

HB	rel. occ.	$d(\text{O} \cdots \text{HO})$	$\angle(\text{OHO})$
bulk			
O3H \cdots O5	34	1.83	157
O2H \cdots O6	34	1.91	158
O3H \cdots O6	0	2.07	148
O6H \cdots O3	14	1.99	154
O6H \cdots O2	12	2.00	154
O6H \cdots O4	6	1.96	157
flat sheets			
O3H \cdots O5	42	1.83	156
O2H \cdots O6	40	1.96	156
O3H \cdots O6	0	2.01	150
O6H \cdots O3	11	2.05	157
O6H \cdots O2	7	2.01	155
O6H \cdots O4	0	2.09	138
rippled sheets			
O3H \cdots O5	35	1.83	157
O2H \cdots O6	34	1.91	161
O3H \cdots O6	1	2.04	149
O6H \cdots O3	23	1.96	152
O6H \cdots O2	8	2.14	155
O6H \cdots O4	0	2.03	137

in both sheet types similarly strong, but the increase of gt and gg conformations in the two sheet types is very different: in flat sheets there are more gg conformations than gt conformations, in rippled sheets there are nearly no gg conformations. Consequently, most hydroxymethyl groups in rippled sheets are involved in inter-chain HBs, whereas in flat sheets they are also involved in inter-sheet HBs. This was also found by Zhang *et al.*[38]. Relative frequencies and geometry parameters of the HBs are given in Table III.

This result diverges considerably from the C13 CP/MAS results that the hydroxymethyl group in $I\alpha$ and $I\beta$ has only the *tg* conformation.[41] Experimentally, two different hydrogen bond networks exist in $I\beta$, but in both networks the hydroxymethyl group has only the *tg* conformation.

In analogy with cellulose $I\beta$, monoclinic cellulose II crystals are made of alternating sheets, but the growth directions of the glucan molecules are reversed in alternating sheets. This allows HBs which do not occur in $I\beta$ and, thus, gives rise to different topologies of the HB network. Inspection of the a,b base plane projection of the cellulose II supercell in figure 6 shows clearly the existence of two sheet types but a distinction between flat and rippled seems to be rather artificial. In the a,b base plane projection of the origin sheets, which are made of the origin units in the unit cell, one can observe a cyclic structure of the inter-chain HBs (sheets 1 and 3 in Figure 6), we find mainly O6H..O2 and little O6H..O3 HBs, the structure is highly regular as nearly all O6H groups are involved in these HBs; the alternating position of the glucose rings that are connected by the inter-chain HBs causes the regular HB network. That means also that in origin sheets there are no O6H..O2 intra-chain HBs; the intra-chain HB O3H...O5 has the same frequency as in $I\beta$.

For the center sheets, which are made of the center units, no cyclic structure of the inter-chain HBs can be seen in the a,b base plane projection. We observe a low regularity in the HB network, which is mainly made from O2H..O6 and O6H..O3 inter-chain HBs, O2H...O6 HBs occur nearly exclusively in the center sheet. Not all O6H..O2 intra-chain HBs are broken and replaced by inter-chain HBs, but the number of O3H...O5 intra-chain HBs is in the center sheets only half of that in the origin sheets, the O3H groups are mainly targets of O6H groups. In center sheets one can also find O2H..O6 intra-chain HBs.

Inter-sheet interaction mainly happens via O2H..O2 HBs with the O2H group from the origin sheet, and O6H..O2 HBs, with the O6H group from the center sheet, but there are also O3H..O6 and O6H..O6 inter-sheet HBs.

Note, the relative occurrences for the bulk in Table IV are not the sum of the occurrences for the layers, the latter do not contain any inter-sheet HBs.

TABLE IV. Distribution of HBs in IIa bulk together with HB parameters. Only bonding atoms with a percentage higher than 0.5 are shown.

HB	rel. occ.	$d(\text{O} \cdots \text{HO})$	$\angle(\text{OHO})$
bulk			
O3H...O5	23	1.94	153.6
O2H...O6	17	1.82	161.3
O6H...O3	17	1.85	156.2
O6H...O2	14	1.83	158.8
O3H...O6	10	2.03	153.0
O6H...O6			
O6H...O4			
O2H...O2	17	1.85	2.830
origin sheet			
O3H...O5	47	1.93	155.4
O2H...O6	1	1.98	154.9
O6H...O3	12	1.94	160.5
O6H...O2	39	1.82	158.9
O3H...O6	1	1.82	157.6
O6H...O6	1	1.98	154.9
O6H...O4			
center sheet			
O3H...O5	21	1.96	149.4
O2H...O6	47	1.81	161.0
O6H...O3	28	1.82	155.0
O6H...O2	1	2.12	150.0
O3H...O6	2	2.02	150.7
O6H...O6			
O6H...O4	0	1.97	139.3

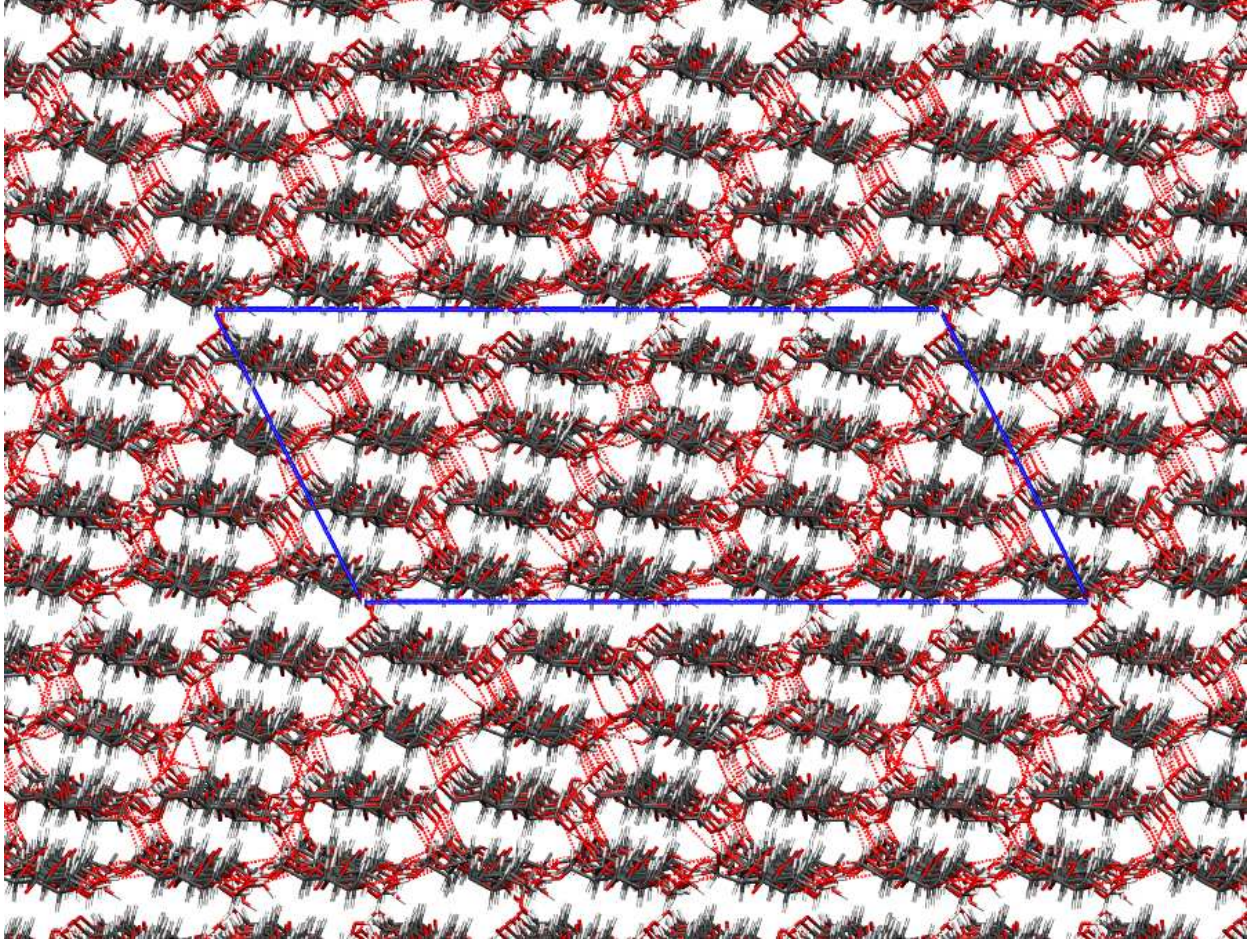


FIG. 6. a,b base plane projection of the cellulose II bulk supercell.

Thermodynamic stability of cellulose bulk

By averaging over configurational energies of the equilibrated systems we get an estimate of the relative thermodynamic stabilities of the different allomorphs. From experiment[17, 42] it is known that heating of cellulose $I\alpha$ will convert it into $I\beta$ and finally into II, but not the other way around. Experimentally, cellulose II is thermodynamically most stable and $I\alpha$ is least stable, our simulations yield the following ordering of the energies per cellobiose unit: $215.0 \text{ kJ mol}^{-1}$ ($I\beta$), $213.8 \text{ kJ mol}^{-1}$ ($I\alpha$), $211.6 \text{ kJ mol}^{-1}$ (IIa) and $210.7 \text{ kJ mol}^{-1}$ (IIb).

Our results corroborate the finding that cellulose II is more stable than cellulose I, the $d(\text{O} \cdots \text{HO})$ distances are in cellulose II shorter than in $I\beta$, indicating that the glucan molecules are closer together and this will increase the stability because the HB and the

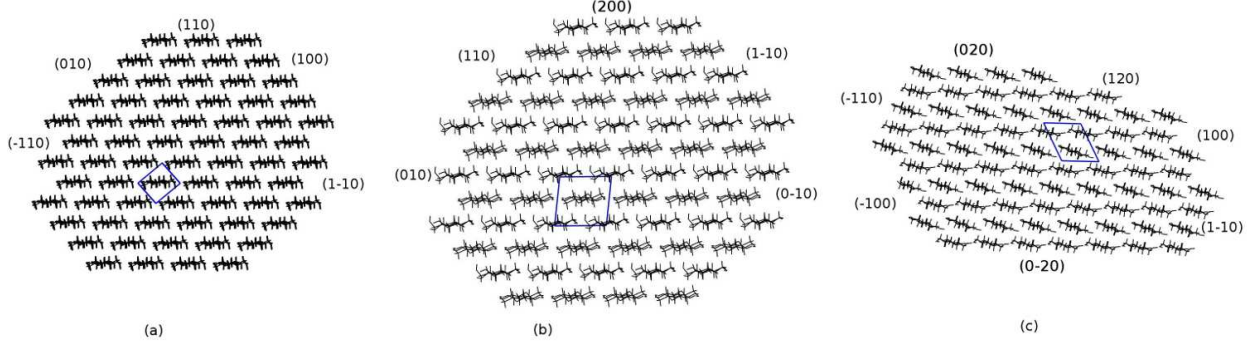


FIG. 7. Schematic structure of cellulose I α (a), I β (b) and II (c) nanocrystallites, exposing different crystal planes.

dispersion interaction will be stronger. According to our quantum chemical calculations dispersion interaction between the chains will be more important than HBs. The expected higher stability of cellulose I β with respect to cellulose I α was, however, not found. We attribute this discrepancy to the fact that our equilibrated I β system is indeed a less stable high temperature system. We are sure that the difference in the stability of cellulose IIa and IIb is caused by the equilibration scheme. Since we were mainly interested in the generation of surfaces of different roughness for the study of the cellulose-water-interface we did not investigate the origin of the difference between the two supercells.

Cellulose/vacuum and cellulose/water interfaces

The aim of this study is to investigate how the properties of the cellulose/water interface depend on the structure of the cellulose surface. Macroscopic cellulose samples, such as fibres or films, are often regarded as being composed of nanocrystallites embedded in amorphous cellulose; in a first approximation, the surface of such a sample can then be seen as a tiling made of many different crystal faces of irregular shape, which are described by the Miller indices of the corresponding crystal planes (see Figure 7). As models for surfaces of the amorphous parts we choose crystal planes with large Miller indices showing large surface roughness. The properties of the macroscopic surface is then an average of the properties of all exposed crystal faces.

It is not possible to investigate the surface properties for all exposed crystal planes, but only for few representatives which differ most strongly in certain properties like surface

roughness, polarity etc. and in the interaction with adsorbates. This approach has also been chosen by e. g. Mazeau and Vergelati[27]. In the $I\alpha$ (100) system the bulk sheets are not parallel to the surface, in the layers parallel to the surface the glucose rings are slanted; in the $I\beta$ (100) the layers are parallel to the surface and at least in the flat sheet also the glucose rings are parallel; in II (010) the layers are made of parallel sheets but the glucose rings are slanted; in II (120), finally, the sheets are not parallel to the surface, the layers are made from glucan molecules that stem alternatively from origin and center sheets and the overall surface shows a zigzag behavior.

The aforementioned molecular dynamics scheme reveals very different degrees of reconstruction for the different surfaces. The $I\alpha$ (100) surface, where the rings of the cellobiose molecules are slanted with respect to the (100) plane, shows high irregularities after equilibration (shown in figure 8b); inter-chain hydrogen bonds become inter-sheet hydrogen bonds and this causes a reduction of the number of hydroxy groups pointing into the vacuum and a strengthening of the bonding between the glucan molecules in the top layer. Not surprising is that the flat (100)/(010) surfaces of cellulose $I\beta$ and II show little reconstruction, this could be different for the more rippled $I\beta$ (200) surface, but we did not investigate it. In spite of the grooved structure of the cellulose II (120) surface we did not find a considerable reconstruction due to vacuum exposure.

To quantify the different roughnesses of the surfaces and thereby the degree of surface reconstruction we adapted a measure which is very common in material science[43]. The R_a value of a surface is defined as follows:

$$R_a = \frac{1}{n} \sum_{i=1}^n |\Delta y_i| \quad \Delta y_i = y_i - \bar{y} \quad (1)$$

Whereas y_i is the absolute height of a surface atom and \bar{y} defines the average surface height. As the average surface height we took the tangential plane to the closed van der Waals spheres of the uppermost layer.

In Table V we show the roughnesses of the four reconstructed surfaces. Roughness is a property of the structure of surfaces, the values from Table V support the classification of $I\beta$ (100) as smooth and of II (120) as rough, that II (010) is much smoother than $I\alpha$ (100) is not that obvious. Interestingly, the difference in roughness between a bulk layer, the surface exposed to vacuum or to a water environment is insignificant compared to the overall difference between the different cellulose types. In addition to the unchanged surface

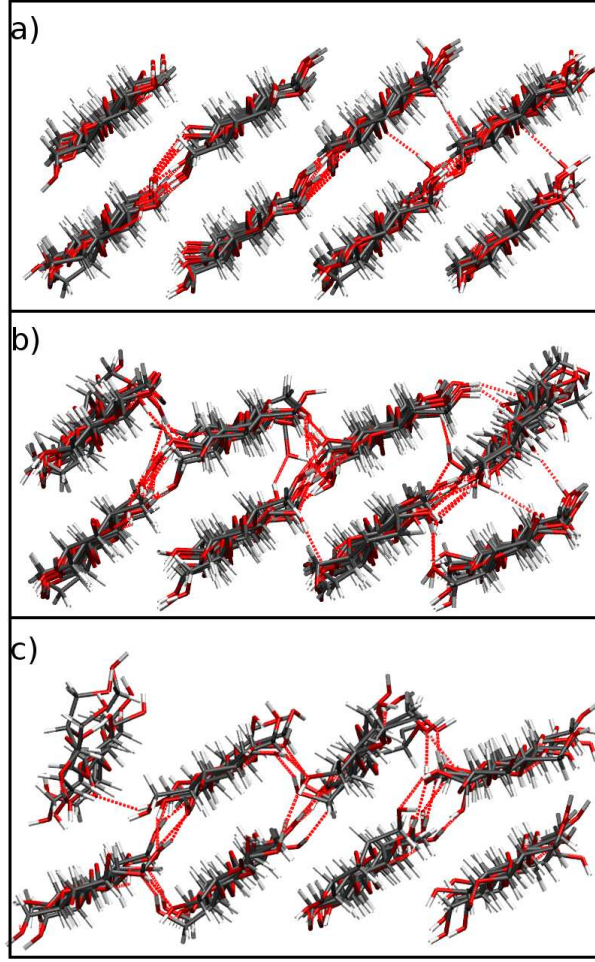


FIG. 8. Cutout of the supercells showing a) parts of two layers of Cellulose I α bulk, b) parts of the first two layers of a Cellulose I α (100) surface exposed to vacuum and c) parts of the first two layers of a Cellulose I α (100) surface exposed to 300 K TIP3P water.

roughness we also were not able to find significant changes of the layer distances orthogonal to the surface. This suggests that at this time scale no drastic changes in the mesoscopic geometric structure of cellulose occurs.

Another frequently used measure for roughness is the standard deviation of the distribution of the absolute heights y_i from the average surface height

$$\tilde{R}_a = \sqrt{\frac{\sum_{i=1}^n (\Delta y_i)^2}{n-1}} \quad (2)$$

The two measures give different roughness values, the \tilde{R}_a values are always larger than the R_a values. For a large number of uniformly distributed random numbers y_i the difference

TABLE V. Roughness R_a [\AA] of cellulose surfaces exposed to vacuum.

Surface	R_a [\AA]
Cellulose I α (100)	0.7418
Cellulose I β (100)	0.5429
Cellulose II (010)	0.5890
Cellulose II (120)	0.8289

is about 16%, for normally distributed random numbers the difference is about 25%. The coordinates of the top layer atoms are neither uniformly nor normally distributed random numbers, therefore, we regard the larger roughness values \tilde{R}_a reported by Mazeau[44] as consistent with our data.

Nonetheless, surface reconstruction at the solid/vacuum interface is accompanied by a significant change of the molecular hydrogen bond network, which can be described by the frequencies of occurrence of the three conformations of the exocyclic C6 group and by the number of hydrogen bonds. The data were obtained from the last 100 ps of the 300 K MD runs.

In Figure 9 the dihedral angles of the exocyclic C6 group are plotted which were measured for the layers in I α (100), but we find for all systems similar distributions with peaks that are easily distinguishable and can be assigned to one of the three dihedral conformations. The area under the peak can be interpreted as the probability of finding this conformation, the relative probabilities for all systems are given in Table VI. The reference data for the crystalline systems with equivalent layers (I α and IIb) are obtained by averaging over all layers, as for cellulose I α and cellulose IIb, or by averaging over the two different kinds of layers, as for cellulose I β and cellulose IIa. The averaged data are always given in line L3, for the systems with two different kinds of equivalent layers, the corresponding data for L1 and L2 are also given.

In the cellulose I α bulk system all layers parallel to the surface show the same relative probabilities for the dihedral conformations within small statistical fluctuations. The small amount of *gg* conformations (6 percent) and the large amount of *gt* (40 percent) and *tg* (54 percent) conformations once again demonstrates that in I α there are nearly no inter-sheet HBs, but many intra- and inter-chain HBs. The alternating layers in the I β system

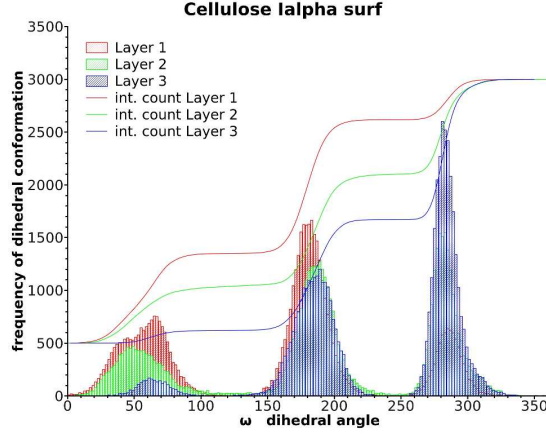


FIG. 9. Representative distributions of C6 dihedral angle conformations for different layers in a Cellulose I α (100) surface exposed to vacuum. Also shown are the integrated occurrence frequencies that are used for analysis.

are identical with the flat and rippled sheets and have rather different distributions of the dihedral conformations with a high frequency of *gg* conformations in the flat sheets (layers 1 and 3) and nearly no *gg* conformations in the rippled sheets (layers 2 and 4), as already discussed above.

In the IIa system again the layers are identical with the sheets and we find accordingly different probability distributions in alternating layers. In the origin sheets (layers 1 and 3) we find again a high number of *gg* conformations indicating that the C6OH groups from these sheets form active inter-sheet HBs whereas little active inter-sheet HBs are made with C6OH groups from center sheets (layers 2 and 4). In the IIb system the layers are made from equal contributions of origin and center glucan molecules and, therefore, all layers show the same probability distribution. The difference between systems IIa and IIb is again demonstrated in the averaged probability distributions which differ mostly in the *gt* and *tg* probabilities.

Now we compare the bulk data with the probabilities for the layers of the cellulose/vacuum interfaces. For I α (100) there is a higher probability to find *gg* and *gt* conformation in the layers near to the surface and a reduced probability to find *tg* conformations. The increase of *gg* conformers corresponds to the increase of inter-sheet HBs between the tilted cellulose chains at the surface. The probability distribution of layer 3 is again very close to the bulk distribution, we interpret this finding as showing that reconstruction of

the $I\alpha$ (100) surfaces is restricted to only few layers.

In cellulose $I\beta$ (100) on the other hand we find only little differences between the probability distribution for the bulk and for the reconstructed surface, because in this system the layers are formed by sheets and the top layer is a flat sheet. Maybe, reconstruction of the (200) surface would result in larger differences at least for the top layer, but we did not investigate this surface.

Although in IIa (010) the layers are identical with sheets, we find strong increase in the probability for gg conformations in the first two layers, the third layer shows again a distribution very similar to that in the bulk. In IIb (120), finally, again only the two top layers are strongly reconstructed, the tg conformations are decreased and the gt conformations are increased.

There is, thus, a very good correspondence of surface roughness and surface reconstruction, the surface with the lowest R_a value shows the least reconstruction, irrespective of whether the layers are sheets or not. This correspondence was also reported by Mazeau *et al.*[44] for cellulose I.

When the vacuum of the solid/vacuum interface is replaced by bulk water we find very different changes of the probability distributions: The changes in the two top layers of $I\alpha$ are much smaller than the changes between the bulk and the solid/vacuum interface, the changes in layer 3 can be neglected. In $I\beta$, on the other hand, we see in the top layer a strong increase of the gg and a strong decrease for the tg conformations, in layer 2 the gt conformations increase in expense of the tg conformations. The changes in layer 3 are again small.

In IIa replacement of the vacuum by water is accompanied by little changes in the probability distributions, in IIb a significant increase of gt in expense of tg conformations is found only in the top layer, the other changes are again rather small.

Summarizing, we found that surfaces that show strong hydrogen bonding reconstruction at the solid/vacuum interface, change little when water replaces the vacuum and vice versa, and, none of the top layers resemble very strongly the corresponding bulk layer hydrogen bond network, that means, there is always a surface reconstruction at an interface, the kind and amount of reconstruction of the cellulose surface depends on the second phase at the interface, the cellulose allomorph and the structure of the crystal plane. Similar results were obtained by Newman and Davidson[45] in a ^{13}C NMR study of the cellulose–water

TABLE VI. C6 dihedral angle distributions for two cellulose interfaces and crystalline bulk. The L stands for the layer in the slab. In systems where the layers are equivalent, the average distribution for the whole slab is shown. Details are given in the main text.

Crystal system	L	crystal bulk	solid/vacuum	solid/water
		$gg : gt : tg$	$gg : gt : tg$	$gg : gt : tg$
Cellulose I α (100)	1		0.34 : 0.51 : 0.16	0.26 : 0.59 : 0.15
	2		0.21 : 0.43 : 0.36	0.18 : 0.48 : 0.34
	3	0.06 : 0.40 : 0.54	0.05 : 0.42 : 0.53	0.00 : 0.46 : 0.54
Cellulose I β (100)	1	0.37 : 0.37 : 0.26	0.48 : 0.27 : 0.25	0.65 : 0.26 : 0.09
	2	0.02 : 0.50 : 0.48	0.02 : 0.62 : 0.36	0.00 : 0.70 : 0.30
	3	0.47 : 0.19 : 0.34	0.55 : 0.13 : 0.32	0.60 : 0.10 : 0.30
	4	0.03 : 0.55 : 0.42		
Cellulose II (010) (IIa)	1	0.22 : 0.74 : 0.04	0.48 : 0.41 : 0.11	0.50 : 0.45 : 0.05
	2	0.08 : 0.27 : 0.65	0.24 : 0.34 : 0.42	0.16 : 0.40 : 0.44
	3	0.21 : 0.76 : 0.03	0.25 : 0.71 : 0.05	0.24 : 0.73 : 0.03
	4	0.06 : 0.26 : 0.68		
Cellulose II (120) (IIb)	1		0.33 : 0.41 : 0.26	0.34 : 0.59 : 0.08
	2		0.30 : 0.57 : 0.13	0.28 : 0.62 : 0.10
	3	0.16 : 0.73 : 0.11	0.19 : 0.73 : 0.09	0.17 : 0.79 : 0.07

interfaces for cellulose I and cellulose II surfaces. From AFM studies of cellulose I α surfaces Baker *et al.*[46] conclude that hydroxymethyl groups will change at the surface from *tg* to *gt* conformation.

The only significant difference between results obtained from the simulations with a 4 layer and an 8 layer supercell, respectively, was found for the distribution of the C6 dihedral angle in the I β bulk which has an a-b-a-b...layer structure. There are, however, large differences in the layers 1 and 3, and 2 and 4, respectively. We find 0.43 : 0.00 : 0.53 : 0.02 for the *gg* conformations, 0.23 : 0.65 : 0.15 : 0.31 for the *gt* conformations and 0.35 : 0.37 : 0.32 : 0.67 for the *tg* conformations. In the 8 layer supercell the differences between different flat and different rippled layers are much smaller, these data are included in table VI; they

TABLE VII. Number of hydrogen bonds within layers per cellobiose unit for the bulk and surface systems, excluding intra-chain $\text{O3H} \cdots \text{O5}$ hydrogen bonds. The L stands for the layer in the slab.

Phase	L	crystal	bulk solid/vacuum	solid/water
Cellulose I α	1	2.10	2.28	1.94
	2	2.01	2.49	2.30
	3	1.99	2.30	2.35
Cellulose I β	1	2.60	2.92	1.92
	2	3.51	3.34	3.19
	3	2.63	2.48	2.49
Cellulose IIa	1	2.12	2.48	2.11
	2	3.01	2.41	2.60
	3	2.09	2.20	2.22
Cellulose IIb	1	2.26	2.68	2.26
	2	2.66	2.41	2.23
	3	2.36	2.20	2.35

are, nevertheless larger than those found for IIb, which has the same layer structure as I β .

The HB networks in cellulose and at the interface are made from more than just the C6OH groups, so we calculated also the average number of all intrachain and interchain HBs, except $\text{O3} \cdots \text{O5}$ HBs per cellobiose unit for each layer in the bulk and interface systems (see Table VII). The analysis did not allow to include intersheet hydrogen bonds, but the unchanged layer distances suggests that the amount of interlayer hydrogen bonding is not strongly affected by interface reconstruction.

Again, we find for the four systems rather different trends: in the top layer of I α , that shows the strongest surface reconstruction, there is a moderate increase of the HBs when going from bulk to solid/vacuum, and a slightly stronger decrease when going to solid/water because the cellulose..water HBs are not counted. In the second and third layer the number of HBs increases with respect to the bulk. Similar trends are found for the I β system.

In the cellulose II systems we observe in the top layer an increase of the number of HBs when going from bulk to solid/vacuum and a strong decrease when going from solid/vacuum to solid/water, there one has about as many HBs as in the crystal layer. In layer 2 of both

interface systems there is a decrease of the number of HBs with respect to the bulk, in layer 3 the resemblance to the bulk is striking.

When a surface is created by cutting a slab out of the crystalline bulk, there will be hydroxy groups in the top layer having no partner to form HBs between the layers (dangling HBs). During the reconstruction of the solid/vacuum interface dangling HBs will be partially converted into inter-chain or maybe also inter-sheet HBs (which were not covered in the analysis of table VII) in the top layer. The additional HBs, due to vacuum exposure one can directly observe for I α (100) in figure 8. In the solid/water interface the former dangling HBs and some of the inter-chain HBs in the top layer form HBs to the water slab. This yields a reduced average amount of HBs within the first cellulose layer. We did not find, however, a significant amount of water molecules penetrating between cellulose chains and diffusion of water molecules into the solid bulk; the formation of hydrated hydroxy groups at the cellulose surface does not seem to be energetically sufficient, at least not in the simulation times used in this study. This leaves us to conclude that pure water at ambient conditions is not able to cause swelling of cellulose at microscopic timescales, but merely wetting.

Structure and dynamics of water at the interface

To investigate the structure of the water slabs at the interfaces we calculated density profiles of the systems orthogonal to the surface, which are shown in Figure 10. The black lines depict the density profiles of the cellulose, the red ones the density of the water.

The cellulose profiles reflect nicely the different layering in the four systems: fine structure is found when the sheets are not parallel to the surface as for I α and IIa, the larger the angle between surface and sheet is, the more structure is found in the profiles. For I β and IIb, where the sheets are parallel to the surface, we just see the peaks of the four and eight layers, respectively, in the systems.

The density profiles of water have an oscillatory form indicating an ordering in the water slab that is not typical for bulk water, the highest density maximum is found near the interfaces. The deviations from the bulk density are strongest for the flat surfaces I β (100) (40 percent) and II (010) (60 percent), and least pronounced for the non-flat surfaces I α (100) (10 percent increase) and II (120) (20 percent increase). The oscillations decay completely within 10 Å at the I α (100) surface the water bulk is undisturbed already after about 4 to

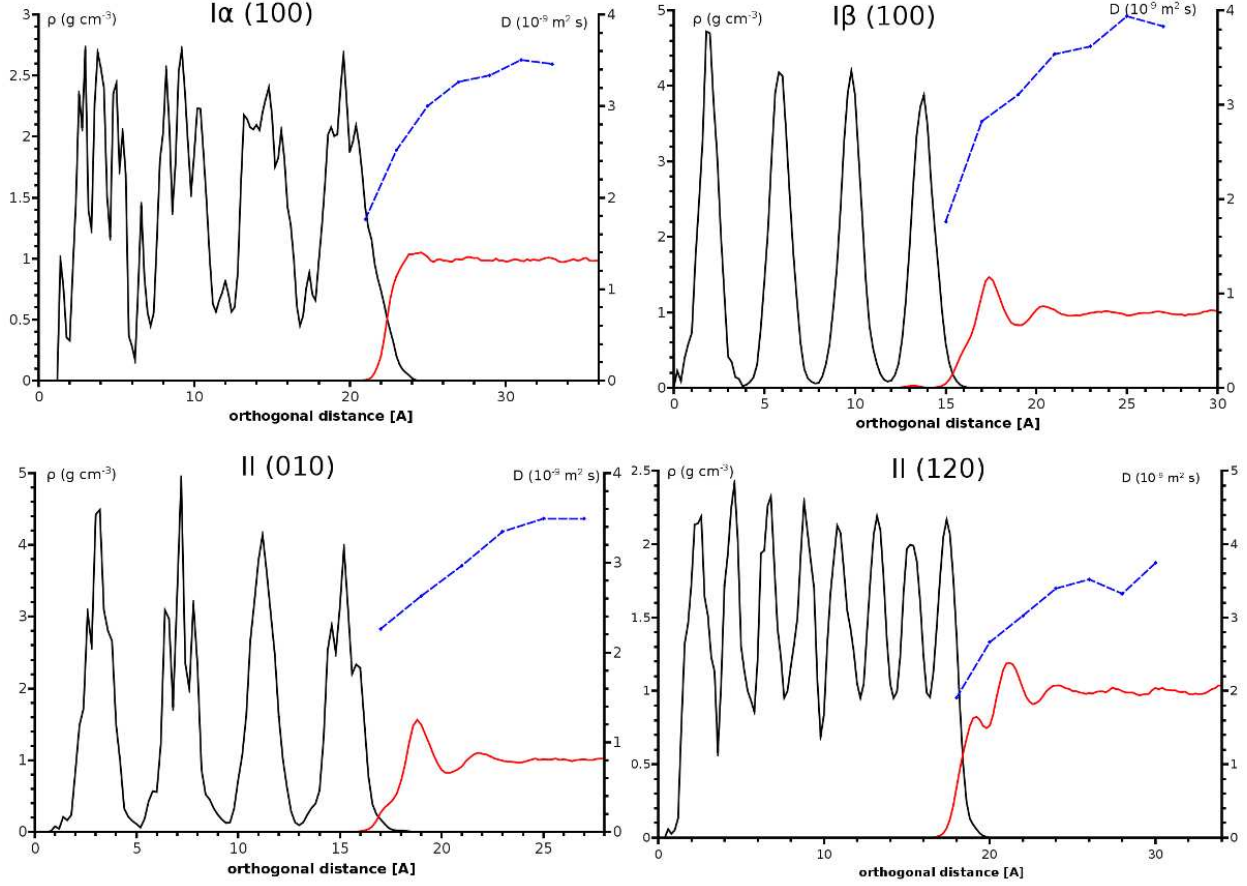


FIG. 10. Density profiles of cellulose-water interfaces, the cellulose profiles (solid left) are for $I\alpha$ (100), $I\beta$ (100), II (010) and II (120), right are the profiles (solid right). The left scale in g cm^{-3} is for the density profiles. Also shown is the diffusion coefficient of water molecules as a function of the surfaces distance (dashed) with the right scale in $10^{-9} \text{ m}^2 \text{ s}^{-1}$.

5 Å.

When placing an undisturbed slab of water onto a cellulose slab, the water molecules rearrange to maximize interactions. We therefore see areas around the cellulose chains, where water molecules adsorb preferentially (around the terminal hydroxy groups) and areas where no hydrogen bonds can be formed, such as around the unpolar hydrogens bonded to the glucan framework. These areas show depletion of water molecules compared to the terminal hydroxy groups (cf. Figure 11). This densification and restructuring of water on the cellulose surfaces happens in a volume of a few Å of vertical distance to the surface. Using a similar reasoning as [24] one can relate the degree of hydrophilicity to the density profile:

TABLE VIII. Diffusion coefficients in m s^{-2} for the first 2 Å thick layer of water in contact with the different cellulose crystal surfaces at 300 K.

Crystal surface	$D \times 10^9 [\text{m s}^{-2}]$
Cellulose I α (100)	1.80(1)
Cellulose I β (100)	2.11(1)
Cellulose II (010)	2.30(1)
Cellulose II (120)	1.90(1)

The more sharp the first peak is, corresponding to a dense layer of water adsorbed on the surface, the more hydrophilic is the surface. However, densification of a water slab above a cellulose surface can also be related to the regularity of the surface. Highly regular surfaces, such as cellulose I β (100) and cellulose II (010), allow a large amount of water molecules within a slab of a certain vertical spacing above the surface. In the case of cellulose I α (and also cellulose II (120) the tilted and slightly irregular chains distribute this effect over a larger vertical range above the surface, although the amount of interacting water molecules may be similar, if not more. The densification of a water slab above a cellulose surface is therefore both, a function of the hydrophilicity and the regularity (roughness) of the surface. We therefore refrain from extrapolating solely from the density profile to the hydrophilicity of the surface, as has been done in literature [24, 40], as long as we don't know in detail how the interaction energy at the water/surface interface depends on the surface morphology. The surface structure of cellulose II (120) surface with eight layers (see Figure 10) allows interaction of water molecules not only with the top layer but also with the second layer, this is reflected in the shifted onset of the water profile which is at the same position as the maximum of the density of the cellulose top layer. Cellulose II (120) should therefore have a larger water accessible surface area and we hoped to observe initial solvation processes. No such processes were observed, however, within the simulation time. This supports the finding that pure water and cellulose do not interact strongly enough to allow easy solubilization at ambient conditions.

Another property that can be used to describe the structure of the water slab at the cellulose surface is the self diffusion coefficient as a function of surface distance. The non-rigid TIP3P water model used in this study yields for bulk water at 300 K a value of $4.0 \cdot 10^{-9} \text{m s}^{-2}$,

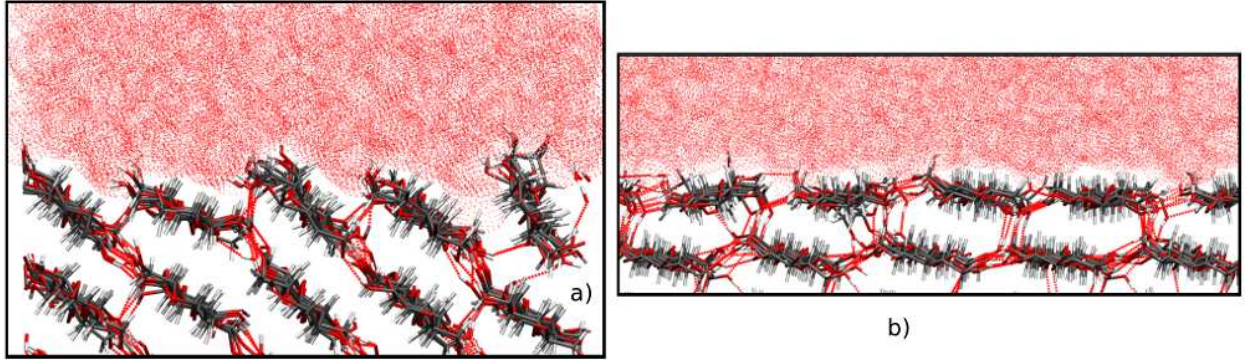


FIG. 11. a,b base plane projection of a) the cellulose I α (100) and b) the cellulose I β (100) slab in contact with water at room temperature and room pressure. Shown are the first layers of cellulose chains as sticks and the adsorbed water molecules in a continuous van der Waals surface representation.

which agrees well with our values at 10 Å, this value is about 50 percent larger than the experimental value of $2.4 \times 10^{-9} \text{ m}^2 \text{ s}^{-1}$ (Refs. [47, 48]), but considerably better than the value that is obtained with the rigid TIP3P model (see Ref [49]), although at considerably higher computational cost. Disregarding the absolute values of the diffusion constant, one can nevertheless obtain an interesting information on the cellulose/water interface: we find a decrease in the diffusion constant from bulk water to water at the interface of about $1.6 \times 10^{-9} \text{ m}^2 \text{ s}^{-1}$ and such a decrease corresponds, according to the data by Harris *et al.*[47], to a decrease of the water temperature of about 30 degrees. The reduction of the diffusion constant at the interface is caused by at least two factors: i) the reduced degrees of freedom of water motion, and ii) the formation of variably dense water regions (‘arches’) at the cellulose/water interface of different stability. One could wonder if the shape of the graphs of the diffusion constant vs. distance from the surface reflects the differences in the water structures as described by the density profiles; it is however not possible to show such a dependence, because the smallest bin size used for the calculation of the self diffusion constant by integration of the velocity autocorrelation function was a slab of 2 Å, which is larger than the strongly fluctuating interface region. In any case, the reduced water mobility and the formation of water structures of different stability at the cellulose surfaces, together with the change in hydrogen bonding patterns can be seen as a main ingredient of wetting of crystalline cellulose. Our results are consistent with the results from a ^2H NMR study[50]

who found three different types of water at the cellulose interface: a strongly bound, rigid water, which cannot crystallize, a highly mobile water, whose motion is hindered due to anisotropic constraints, so that it can only undergo fast 180 flips around their bisector axis, and finally the mobile water that can perform isotropic motions. This agrees also very well with the results from ^1H and ^{13}C solid state NMR results by Taylor *et al.*[51] that moisture adsorbed at cellulose surfaces has different correlation times.

As shown by Vega *et al.* [49], the choice of the water model crucially influences the properties of liquid water and water steam. It should not be much of a surprise if the water model also influences the dynamical properties of interfaces. Dynamical observables might depend strongly on how balanced the force fields used for the cellulose and water description are.

IV. CONCLUSION

Cellulose is a biological material of immense structural complexity. In this work we approached this material starting from idealized crystalline bulk structures. We investigated the structure of different bulk crystals that allows a somewhat closed view. It is often claimed in literature that the attractive interaction between $\text{I}\alpha$ sheets is mainly dispersion interaction, whereas $\text{I}\beta$ and II show strong polar intersheet interactions; it should be clear that dispersion interaction is important for all kind of interfaces, irrespective of whether there are hydrogen bonds or not. Due to similar distances in our classical dynamical approach we always find a constant background of dispersion interaction for all crystal systems. Of course, one should know how much of the stabilization energy is dispersion energy and how much is, say, hydrogen bonding energy, but to do this quantum theoretical methods must be used. Work is in progress in our group to investigate the stabilization of chains in sheets, or between sheets in bulk, and to calculate the contribution of dispersion interaction to stabilize these structures.

Knowledge of the reorganization of these bulk materials on interfaces is a basic prerequisite to understand more complex interactions that would involve ions, restructuring at non-standard conditions and, most interestingly, adsorption of complex nanostructured materials. When cellulose surface slabs are allowed to reconstruct, the degree of reconstruction depends strongly on the allomorph and the type of crystal plane that is chosen as slab sur-

face. As a main result we find that within nanoseconds no significant mesoscopic structural changes, such as changes in layer distances, chain tilting or strong irregularities, occur. This might lead to the conclusion that cellulose surfaces in contact with vacuum or water show no restructuring at all. A detailed view on the molecular structure and the hydrogen bonding network reveals substantial restructuring, although only for the first few layers.

Adsorption of water on cellulose surfaces cannot be solely explained with the formation of hydrogen bonds between water molecules and oxygen containing groups at the surface, as in the bulk, dispersion interaction must be considered as well. And to find out, whether the interaction between glucan molecules, that is hydrogen bonds and dispersion interaction, are quantitatively correct described with force fields and water models, comparative quantum theoretical investigations are needed, specifically addressing the hydrogen bond strength and amount of dispersion interaction between the chains in cellulose. Such investigations are under way in our group (Hoja, Grossar, Maurer and Sax, to be published). The results presented here point to different wettability of different cellulose surfaces, due to a different ratio of polar and unpolar moieties. This observation has already been made in recent studies[20, 40]. We can confirm those results and augment them with the observation that even loosely packed high index surfaces, such as Cellulose II (120) do not allow significant solvation and swelling within a mesoscopic time frame. We further found hints that water applied to surfaces that were optimized against vacuum can partially reverse the surface reconstruction, even though they did not insert between cellulose sheets, that were previously reconstructed against vacuum. Anyhow, we did not find that swelling of cellulose can be caused by pure water.

ACKNOWLEDGMENTS

The authors like to acknowledge financial support by the European Union Framework Program 7 Project SURFUNCELL, Grant agreement No.: 214653, and the helpful comments of an unknown reviewer.

[1] A. O’Sullivan, “Cellulose: the structure slowly unravels,” *Cellulose*, vol. 4, pp. 173–207, 1997.

[2] S. J. Eichhorn, A. Dufresne, M. Aranguren, N. E. Marcovich, J. R. Capadona, S. J. Rowan,

- C. Weder, W. Thielemans, M. Roman, S. Renneckar, W. Gindl, S. Veigel, J. Keckes, H. Yano, K. Abe, M. Nogi, A. N. Nakagaito, A. Mangalam, J. Simonsen, A. S. Benight, A. Bismarck, L. A. Berglund, and T. Peijs, "Review: current international research into cellulose nanofibres and nanocomposites," *J. Mater. Sci.*, vol. 45, pp. 1–33, Sept. 2010.
- [3] S. Hornig and T. Heinze, "Efficient approach to design stable water-dispersible nanoparticles of hydrophobic cellulose esters.," *Biomacromol.*, vol. 9, pp. 1487–1492, May 2008.
- [4] F. J. Kolpak and J. Blackwell, "Determination of the structure of cellulose II.," *Macromol.*, vol. 9, no. 2, pp. 273–278, 1976.
- [5] M. Wada, H. Chanzy, Y. Nishiyama, and P. Langan, "Cellulose III Crystal Structure and Hydrogen Bonding by Synchrotron X-ray and Neutron Fiber Diffraction," *Macromol.*, vol. 37, no. 23, pp. 8548–8555, 2004.
- [6] K. H. Gardner and J. Blackwell, "The structure of native cellulose," *Biopolymers*, vol. 13, no. 10, pp. 1975–2001, 1974.
- [7] K. H. Gardner and J. Blackwell, "The hydrogen bonding in native cellulose," *Biochim. Biophys. Acta*, vol. 343, no. 1, pp. 232–237, 1974.
- [8] P. Langan, Y. Nishiyama, and H. Chanzy, "A Revised Structure and Hydrogen-Bonding System in Cellulose II from a Neutron Fiber Diffraction Analysis," *J. Am. Chem. Soc.*, vol. 121, pp. 9940–9946, Nov. 1999.
- [9] Y. Nishiyama, P. Langan, and H. Chanzy, "Crystal Structure and Hydrogen-Bonding System in Cellulose I β from Synchrotron X-ray and Neutron Fiber Diffraction," *J. Am. Chem. Soc.*, vol. 124, no. 31, pp. 9074–9082, 2002.
- [10] Y. Nishiyama, J. Sugiyama, H. Chanzy, and P. Langan, "Crystal structure and hydrogen bonding system in cellulose I(alpha) from synchrotron X-ray and neutron fiber diffraction.," *J. Am. Chem. Soc.*, vol. 125, pp. 14300–14306, Nov. 2003.
- [11] S. Perez, M. Kouwijzer, K. Mazeau, and S. Balling Engelsen, "Modeling polysaccharides: Present status and challenges," *J. Mol. Graph.*, vol. 14, pp. 307–321, Dec. 1996.
- [12] L. M. J. Kroon-Batenburg and J. Kroon, "The crystal and molecular structures of cellulose I and II," *Glycoconjugate J.*, vol. 14, pp. 677–690, Aug. 1997.
- [13] K. Mazeau and L. Heux, "Molecular Dynamics Simulations of Bulk Native Crystalline and Amorphous Structures of Cellulose," *J. Phys. Chem. B*, vol. 107, pp. 2394–2403, Mar. 2003.
- [14] R. J. Vietor, K. Mazeau, M. Lakin, and S. Perez, "A priori crystal structure prediction of

- native celluloses,” *Biopolymers*, vol. 54, no. 5, pp. 342–354, 2000.
- [15] A. P. Heiner, J. Sugiyama, and O. Teleman, “Crystalline cellulose I [α] and I [β] studied by molecular dynamics simulation,” *Carbohydr. Res.*, vol. 273, pp. 207–223, Aug. 1995.
 - [16] M. Bergenstrahle, L. A. Berglund, and K. Mazeau, “Thermal response in crystalline I β cellulose: a molecular dynamics study,” *J. Phys. Chem. B*, vol. 111, pp. 9138–9145, Aug. 2007.
 - [17] L. M. J. Kroon-Batenburg, B. Bouma, and J. Kroon, “Stability of Cellulose Structures Studied by MD Simulations. Could Mercerized Cellulose II Be Parallel?,” *Macromol.*, vol. 29, pp. 5695–5699, Jan. 1996.
 - [18] B. Hardy and A. Sarko, “Molecular dynamics simulations and diffraction-based analysis of the native cellulose fibre: structural modelling of the I- α and I- β phases and their interconversion,” *Polymer*, vol. 37, pp. 1833–1839, May 1996.
 - [19] S. J. Eichhorn, R. J. Young, and G. R. Davies, “Modeling crystal and molecular deformation in regenerated cellulose fibers,” *Biomacromol.*, vol. 6, no. 1, pp. 507–513, 2005.
 - [20] J. F. Matthews, C. E. Skopec, P. E. Mason, P. Zuccato, R. W. Torget, J. Sugiyama, M. E. Himmel, and J. W. Brady, “Computer simulation studies of microcrystalline cellulose I β ,” *Carbohydr. Res.*, vol. 341, pp. 138–152, 2006.
 - [21] T. Yui, S. Nishimura, S. Akiba, and S. Hayashi, “Swelling behavior of the cellulose I β crystal models by molecular dynamics,” *Carbohydr. Res.*, vol. 341, pp. 2521–2530, Nov. 2006.
 - [22] T. Yui and S. Hayashi, “Molecular dynamics simulations of solvated crystal models of cellulose I- α and III,” *Biomacromol.*, vol. 8, pp. 817–824, 2007.
 - [23] A. P. Heiner and O. Teleman, “Interface between Monoclinic Crystalline Cellulose and Water: Breakdown of the Odd/Even Duplicity,” *Langmuir*, vol. 13, pp. 511–518, Feb. 1997.
 - [24] O. Biermann, E. Hädicke, S. Koltzenburg, and F. Müller-Plathe, “Hydrophilicity and Lipophilicity of Cellulose Crystal Surfaces,” *Angew. Chem. Int. Ed.*, vol. 40, no. 20, pp. 3822–3825, 2001.
 - [25] K. Mazeau and A. Rivet, “Wetting the (110) and (100) surfaces of I β cellulose studied by molecular dynamics,” *Biomacromol.*, vol. 9, pp. 1352–4, Apr. 2008.
 - [26] M. Bergenstrahle, K. Mazeau, and L. Berglund, “Molecular modeling of interfaces between cellulose crystals and surrounding molecules: Effects of caprolactone surface grafting,” *Eur. Polym. J.*, vol. 44, pp. 3662–3669, Nov. 2008.

- [27] K. Mazeau and C. Vergelati, “Atomistic Modeling of the Adsorption of Benzophenone onto Cellulosic Surfaces,” *Langmuir*, vol. 18, pp. 1919–1927, Mar. 2002.
- [28] E. Kontturi, M. Suchy, P. Penttilä, B. Jean, K. Pirkkalainen, M. Torkkeli, and R. Serimaa, “Amorphous characteristics of an ultrathin cellulose film,” *Biomacromol.*, vol. 12, no. 2, pp. 770–777, 2011.
- [29] C. Aulin, S. Ahola, P. Josefsson, T. Nishino, Y. Hirose, M. Osterberg, and L. Wagberg, “Nanoscale cellulose films with different crystallinities and mesostructures—their surface properties and interaction with water,” *Langmuir*, vol. 25, no. 13, pp. 7675–7685, 2009.
- [30] W. Smith, I. T. Todorov, and M. Leslie, “The DL_POLY molecular dynamics package,” *Z. Kristallogr.*, vol. 220, no. 5-6, pp. 563–566, 2005.
- [31] K. N. Kirschner, A. B. Yongye, S. M. Tschampel, J. Gonzalez-Outeirino, C. R. Daniels, B. L. Foley, and R. J. Woods, “GLYCAM06: a generalizable biomolecular force field. Carbohydrates,” *J. Comput. Chem.*, vol. 29, no. 4, pp. 622–655, 2008.
- [32] W. L. Jorgensen, J. Chandrasekhar, J. D. Madura, R. W. Impey, and M. L. Klein, “Comparison of simple potential functions for simulating liquid water,” *J. Chem. Phys.*, vol. 79, no. 2, pp. 926–935, 1983.
- [33] D. A. Case, T. E. Cheatham, T. Darden, H. Gohlke, R. Luo, K. M. Merz, A. Onufriev, C. Simmerling, B. Wang, and R. J. Woods, “The Amber biomolecular simulation programs,” *J. Comput. Chem.*, vol. 26, no. 16, pp. 1668–1688, 2005.
- [34] P. Sherwood, A. de Vries, M. Guest, G. Schreckenbach, C. Catlow, S. French, A. Sokol, S. Bromley, W. Thiel, A. Turner, S. Billeter, F. Terstegen, S. Thiel, S. Kendrick, J. Kendrick, S. Rogers, J. Casci, M. Watson, F. King, E. Karlsen, M. Sjøvoll, A. Fahmi, A. Schäfer, and L. C, “QUASI: A general purpose implementation of the QM/MM approach and its application to problems in catalysis,” *J. Mol. Struct.: THEOCHEM*, vol. 632, no. 1-3, pp. 1–28, 2003.
- [35] T. G. A. Youngs, “Aten - An application for the creation, editing, and visualization of coordinates for glasses, liquids, crystals, and molecules,” *J. Comput. Chem.*, vol. 31, no. 3, pp. 639–648, 2010.
- [36] W. Humphrey, A. Dalke, and K. Schulten, “VMD – Visual Molecular Dynamics,” *J. Molec. Graphics*, vol. 14, pp. 33–38, 1996.
- [37] L. Martinez, R. Andrade, E. G. Birgin, and J. M. Martinez, “PACKMOL: A Package for Building Initial Configurations for Molecular Dynamics Simulations,” *J. Comput. Chem.*, vol. 30,

- pp. 2157–2164, 2009.
- [38] Q. Zhang, V. Bulone, H. Ågren, and Y. Tu, “A molecular dynamics study of the thermal response of crystalline cellulose I β ,” *Cellulose*, vol. 18, no. 2, pp. 207–221, 2011.
 - [39] P. Chen, Y. Nishiyama, and K. Mazeau, “Torsional Entropy at the Origin of the Reversible Temperature-Induced Phase Transition of Cellulose,” *Macromol.*, vol. 45, no. 1, pp. 362–368, 2012.
 - [40] A. P. Heiner, L. Kuutti, and O. Teleman, “Comparison of the interface between water and four surfaces of native crystalline cellulose by molecular dynamics simulations,” *Carbohydr. Res.*, vol. 306, pp. 205–220, 1998.
 - [41] M. Wada, L. Heux, and J. Sugiyama, “Polymorphism of Cellulose I Family: Reinvestigation of Cellulose IV $_I$,” *Biomacromol.*, vol. 5, pp. 1385–1391, 2004.
 - [42] H. Yamamoto, F. Horii, and H. Odani, “Structural-Changes of native cellulose crystals induced by annealing in aqueous alkaline and acidic solutions at high-temperatures,” *Macromol.*, vol. 22, no. 10, pp. 4130–4132, 1989.
 - [43] E. P. Degarmo, J. T. Black, and R. A. Kohser, *Materials and Processes in Manufacturing*. Wiley, 9th ed., 2003.
 - [44] K. Mazeau, “On the external morphology of native cellulose microfibrils,” *Carbohydr. Polym.*, vol. 84, no. 4, pp. 524–532, 2011.
 - [45] R. H. Newman and T. C. Davidson, “Molecular conformations at the cellulose–water interface,” *Cellulose*, vol. 11, pp. 23–32, 2004.
 - [46] A. A. Baker, W. Helbert, J. Sugiyama, and M. J. Miles, “New Insight into Cellulose Structure by Atomic Force Microscopy Shows the I α Crystal Phase at Near-Atomic Resolution,” *Biophysical J.*, vol. 79, pp. 1139–1145, 2000.
 - [47] K. R. Harris and L. A. Woolf, “Pressure and temperature dependence of the self diffusion coefficient of water and oxygen-18 water,” *J. Chem. Soc., Faraday Trans. 1 F*, vol. 76, pp. 377–385, 1980.
 - [48] M. Holz, S. Heil, and A. Sacco, “Temperature-dependent self-diffusion coefficients of water and six selected molecular liquids for calibration in accurate ^1H NMR PFG measurements,” *Phys. Chem. Chem. Phys.*, vol. 2, pp. 4740–4742, 2000.
 - [49] C. Vega, J. Abascal, M. Conde, and J. Aragones, “What ice can teach us about water interactions: a critical comparison of the performance of different water models,” *Faraday Discuss.*,

- vol. 141, pp. 251–276, 2009.
- [50] D. Radloff, C. Boeffel, and H. W. Spiess, “Cellulose and Cellulose/Poly(vinyl alcohol) Blends. 2. Water Organization Revealed by Solid-State NMR Spectroscopy,” *Macromol.*, vol. 29, no. 5, pp. 1528–1534, 1996.
- [51] R. E. Taylor, A. D. French, G. R. Gamble, D. S. Himmelsbach, R. D. Stipanovic, D. P. Thibodeaux, P. J. Wakelyn, and C. Dybowski, “ ^1H and ^{13}C solid state NMR of *Gossypium barbadense* (Pima) cotton,” *J. Mol. Struct.*, vol. 878, pp. 177–184, 2008.